International Journal of Nanomedicine

Dovepress

open access to scientific and medical research

Open Access Full Text Article

ORIGINAL RESEARCH

Cell-delivered magnetic nanoparticles caused hyperthermia-mediated increased survival in a murine pancreatic cancer model

This article was published in the following Dove Press journal:
International Journal of Nanomedicine
17 January 2012
Number of times this article has been viewed

Matthew T Basel[1]
Sivasai Balivada[1]
Hongwang Wang[2]
Tej B Shrestha[1]
Gwi Moon Seo[1]
Marla Pyle[1]
Gayani Abayaweera[2]
Raj Dani[2]
Olga B Koper[2]
Masaaki Tamura[1]
Viktor Chikan[2]
Stefan H Bossmann[2]
Deryl L Troyer[1]

[1]Department of Anatomy and Physiology, College of Veterinary Medicine, [2]Department of Chemistry, Kansas State University, Manhattan, KS, USA

Abstract: Using magnetic nanoparticles to absorb alternating magnetic field energy as a method of generating localized hyperthermia has been shown to be a potential cancer treatment. This report demonstrates a system that uses tumor homing cells to actively carry iron/iron oxide nanoparticles into tumor tissue for alternating magnetic field treatment. Paramagnetic iron/iron oxide nanoparticles were synthesized and loaded into RAW264.7 cells (mouse monocyte/macrophage-like cells), which have been shown to be tumor homing cells. A murine model of disseminated peritoneal pancreatic cancer was then generated by intraperitoneal injection of Pan02 cells. After tumor development, monocyte/macrophage-like cells loaded with iron/iron oxide nanoparticles were injected intraperitoneally and allowed to migrate into the tumor. Three days after injection, mice were exposed to an alternating magnetic field for 20 minutes to cause the cell-delivered nanoparticles to generate heat. This treatment regimen was repeated three times. A survival study demonstrated that this system can significantly increase survival in a murine pancreatic cancer model, with an average post-tumor insertion life expectancy increase of 31%. This system has the potential to become a useful method for specifically and actively delivering nanoparticles for local hyperthermia treatment of cancer.

Keywords: cytotherapy, pancreatic cancer, disseminated peritoneal carcinomatosis, targeted magnetic hyperthermia, nanoparticles

Introduction

Pancreatic cancer is known to be one of the most lethal forms of cancer with 5-year survival rates of less than 5%.[1] Discovering new methods for successfully treating pancreatic cancer is a virtual necessity for combating this disease.

Hyperthermia has been a cancer therapy method for decades. Tumors have been shown to have increased susceptibility to elevated temperature compared to healthy tissue due to their increased rate of cell cycling, increased hypoxia, poor fluid exchange, and increased acidity.[2,3] Whole body hyperthermia is used clinically to take advantage of this differential toxicity to treat cancer. Unfortunately, "extreme" whole body hyperthermia (>41.5°C), which elevates core temperatures to the level where direct thermal toxicity is observed, can cause severe side effects, which may limit its usefulness.[4–8] Fever-level whole body hyperthermia (~39°C–41°C) can mitigate many of these side effects and has potential to be an effective cancer treatment, but this lower heat level is thought, primarily, to stimulate the immune system and the benefits of direct thermal toxicity are reduced.[9,10] Generating localized hyperthermia at the cancer site could alleviate many of the side effects associated with whole body hyperthermia while still taking advantage of the thermal susceptibility of tumors.

Correspondence: Matthew T Basel
1600 Denison Ave, 228 Coles Hall, Kansas State University, Manhattan, KS 66506, USA
Tel +1 785 532 4519
Email mbasel@vet.ksu.edu

One particularly promising method for generating localized hyperthermia is using magnetic nanoparticles to absorb energy from alternating magnetic fields (AMF) and converting this energy into heat. This method is promising because the body is extremely permeable to AMF, which itself produces no known effects in the body. For magnetic hyperthermia, superparamagnetic iron oxide nanoparticles are usually used for absorbing the magnetic field. Core-shell iron/iron oxide nanoparticles have advantages over the simple iron oxide nanoparticles because the solid iron core gives a much stronger magnetization to the nanoparticle, allowing the nanoparticle to absorb the AMF more efficiently. Iron/iron oxide magnetic nanoparticles have also been shown to be safe in vivo and can show very low toxicity when administered in vivo.[11–14] Only at the location of the magnetic nanoparticles is AMF energy absorbed and converted to heat. By specifically delivering the magnetic nanoparticles to the tumor site, localized hyperthermia can be created.[15–17] Using magnetic nanoparticles for generating localized hyperthermia has proven successful,[18–28] and there are several clinical trials using injectable magnetic nanoparticles combined with AMF for tumor treatment. Current methods of delivering magnetic nanoparticles for localized hyperthermia depend on direct injection of milligram amounts of magnetic nanoparticles into the tumor site.[18–27] Although practical for easily accessible tumors, this direct injection limits the usefulness of magnetic nanoparticle-generated localized hyperthermia for deep tumors, locally or systemically metastatic tumors, and other diffuse tumors.

A recent method for targeting cancer therapy is using cytotherapy. Cytotherapy utilizes delivery cells, such as stem cells or other cells, to carry a payload into the tumor site.[29–37] Cytotherapy-directed hyperthermia has been successfully demonstrated to attenuate mouse melanomas.[38]

Monocytes and macrophages are known to infiltrate tumor sites and thus could act as cytotherapeutic drug delivery vehicles.[39,40] Several recent studies have demonstrated the feasibility of delivering therapeutics to tumors using monocytes or macrophages, including targeting liposomes containing fluorescent markers to gastric tumors,[41] targeting adenovirus to prostate tumors,[42] and targeting gold nanoshells to gliomas.[43]

This report demonstrates a system that uses monocyte-like tumor homing cells to deliver magnetic nanoparticles directly into the tumor tissue. It was demonstrated that RAW264.7 cells (monocyte/macrophage-like cells, Mo/Ma, ATCC TIB-71) specifically infiltrate pancreatic tumors when injected intraperitoneally (i.p.) without infiltrating other organs. These cells were loaded with magnetic nanoparticles in order to deliver the magnetic nanoparticles specifically to the tumors for localized hyperthermia. To test this system, a murine model of disseminated peritoneal carcinomatosis of the pancreas was generated by injecting Pan02 cells i.p. into C57BL/6 mice.[44] Magnetic nanoparticle-loaded Mo/Ma were then injected and allowed to infiltrate the tumor tissue. Three days after Mo/Ma injection, mice were treated with AMF. This treatment system significantly increased the survival time of mice bearing i.p. pancreatic tumors, with an average lifespan increase post-tumor injection of 31%.

Materials and methods

Reagents and cells

C57BL/6 mice (11 weeks old) were purchased from Charles River Laboratories (Wilmington, MA). RAW264.7 cells were purchased from ATCC (Manassas, VA), authenticated by ATCC using cell morphology, karyotype analysis, and cytochrome C oxidase analysis, and cultured for less than 6 months. Pan02 cells were obtained from the Division of Cancer Treatment and Diagnosis Tumor Repository (National Cancer Institute, Frederick, MD), authenticated by the National Cancer Institute using cell morphology, and cultured for less than 6 months. Fetal bovine serum, neocuproine, ascorbic acid, ammonium acetate, concentrated hydrochloric acid, tetrahydrofuran, succinic anhydride, dopamine hydrochloride, di-tert-butyl dicarbonate, 1,2-dichloroethane, 4-dimethylaminopyridine, trifluoroacetic acid, tetraethylene glycol, Hoechst 33258, PKH26, and benzyl bromide were purchased from Sigma-Aldrich Corporation (St Louis, MO). Roswell Park Memorial Institute (RPMI) medium, Geneticin® (G418), hygromycin B, and penicillin-streptomycin were purchased from Invitrogen (Carlsbad, CA). Thiazolyl blue and sodium dodecyl sulfate were purchased from Thermo Fisher Scientific (Pittsburgh, PA). Ferrozine reagent (FerroZine®) was purchased from Hach Company (Loveland, CO).

Cell culture

Double-stable RAW264.7 cells were cultured in RPMI medium containing 10% fetal bovine serum, 100 μg/mL G418, and 100 μg/mL hygromycin in a 37°C humidified incubator with 5% carbon dioxide. Pan02 cells were cultured in Roswell Park Memorial Institute with 10% fetal bovine serum and 1 × penicillin-streptomycin in a 37°C humidified incubator with 5% carbon dioxide.

Synthesis of nanoparticles

The synthesis of iron/iron oxide nanoparticles has been reported by direct reduction of iron chloride in aqueous

nanodroplets in reverse micelles (cetyltrimethylammonium bromide, n-octane, tert-butyl).[45–47] In order to obtain much better defined conditions, the synthesis of iron oxide nanoparticles was performed prior to its reduction to iron(0) by adding defined amounts of ammonia to the reverse micelles under an argon atmosphere. Due to the change in pH in the nanodroplets (from <2 to >7), iron oxide nanoparticles were formed, which can be harvested by centrifugation (at 10,000 rpm for 10 minutes), redispersed in ethanol at 0°C, and then reduced by adding solid sodium-borohydride. The last step consisted of dispersing iron/iron oxide nanoparticles in water (argon atmosphere) and spinning off the nanoparticles (at 15,000 rpm for 5 minutes). This step was repeated three times to remove all the byproducts of the reduction process.[48] After sodium-borohydride reduction, each nanorod contained an iron(0) core, as identified by high-resolution transmission electron microscope (lattice constant: 0.287 nm).[49]

The ligand 3-(3,4-dihydroxyphenethylcarbamoyl) propanoic acid tetraethylene glycol ester (ligand 1) was synthesized from 3-(3,4-dihydroxyphenethylcarbamoyl) propanoic acid; 3-(3,4-dihydroxyphenethylcarbamoyl) propanoic acid was synthesized by multistep protection and deprotection of dopamine hydrochloride, followed by reacting with succinic anhydride, 1,2-dichloroethane coupling with tetraethylene glycol, and palladium on carbon-catalyzed hydrogenation deprotecting benzyl group according to published methods.[50,51] Ligand 1 (40 mg) was dissolved in 5 mL tetrahydrofuran, and 20 mg iron/iron oxide nanoparticles were added. After sonicating for 60 minutes, the nanoparticles were precipitated by centrifugation (15,000 rpm, 5 minutes) and washed with 3.0 mL of tetrahydrofuran for ten washing-centrifugation/redispersion cycles (Figure 1A). After drying in high vacuum, 18 mg of surface-modified nanoparticles were obtained. Transmission electron microscopy (Philips CM 100, 100kV and FEI Tecnai F20XT, 200kV; FEI, Hilsboro, OR) imaging showed that the resulting nanoparticles were rod-like in shape (Figure 1B–D).

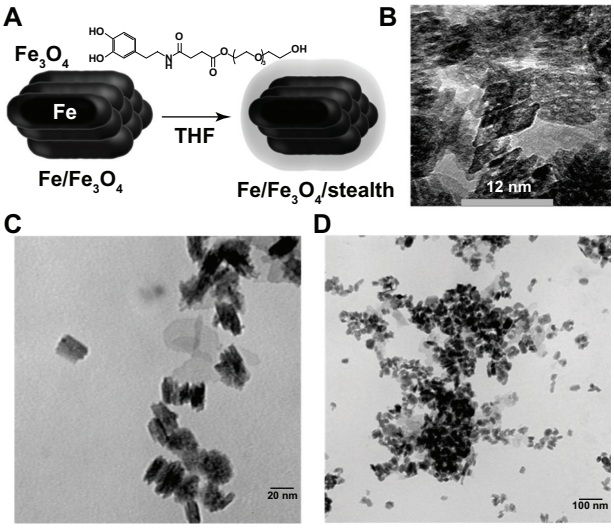

Figure 1 Nanoparticle synthesis. (**A**) Core/shell iron/iron oxide nanoparticles were synthesized and then coated in a dopamine based stealth ligand. (**B**–**D**) Transmission electron microscopic image of obtained particles showing bunched rods.
Abbreviations: Fe, iron; Fe_3O_4, iron oxide; THF, tetrahydrofuran.

Loading Mo/Ma with nanoparticles and determination of iron loading concentration

To determine the optimal concentration for nanoparticle loading, Mo/Ma were plated in 24-well plates and allowed to come to 70% confluency. Medium was removed from the cells and fresh medium was added containing 0–200 μg/mL iron from the nanoparticles. Sixteen hours later the medium was removed, the cells were washed with phosphate buffered saline (PBS), and fresh medium was added. Loading confirmation and concentration were obtained by lifting the cells and running a ferrozine assay for iron content. The percentage of cells loaded was measured using flow cytometry. Cytotoxicity was measured using 3-(4,5-dimethylthiazol-2-yl)-2,5-diphenyltetrazolium bromide (MTT) assay.

For injections, Mo/Ma were cultured to 70% confluency in T75 flasks. Sixteen hours before using the cells, cells for groups three and five (see below) were given nanoparticles containing 373 μg (37.3 μg/mL) of iron added to the media in 100 μL of PBS and mixed well. At the same time, cells for groups one, two, and four were given 100 μL of PBS. The next morning, the medium was removed, the cells were washed with PBS, and fresh medium was added. The cells were lifted by scraping and counted in a hemocytometer (Fisher Scientific, St Louis, MO) using trypan blue. The correct cell density was attained by spinning the cells in 15 mL conical tubes at 1000 rpm for 5 minutes and resuspending in the correct volume of PBS to give 2,000,000 cells in 100 μL.

Ferrozine assay

To determine the iron content of the nanoparticle solutions and the nanoparticle-loaded cells, a ferrozine assay for iron was carried out. Ferrozine reagent was prepared by dissolving 9.7 g ammonium acetate and 8.8 g of ascorbic acid in 10 mL of water. Ferrozine (80 mg) and neocuproine (80 mg) were added to the solution and water was added to bring the total volume to 25 mL. The sample to be measured (either cell suspension or nanoparticle solution) was diluted to appropriate concentrations in deionized water.

For cell suspension samples, the cells were counted on a hemocytometer using trypan blue before dilution. The diluted sample (2 mL) was then placed in a test tube and 0.5 mL of 1.2 M hydrochloric acid and 0.2 mL of 2M ascorbic acid were added. The sample was then vortexed and incubated at 70°C for 1 hour. The ferrozine reagent (0.2 mL) was then added to the test tube and the sample was incubated at room temperature for 30 minutes. A standard curve was also prepared with 0, 0.1, 0.2, 0.5, 1, 2, and 5 μg/mL iron and treated in the same way. After the second incubation, the absorbance at 562 nm of the standard curve and the samples was measured. The $absorbance_{562\ nm}$ versus iron concentration was plotted for the standard curve and the sample concentration was determined.

Flow cytometry

To find the percent of magnetic nanoparticle-loaded Mo/Ma, cells were treated with nanoparticles containing 5, 10, 15, 20, or 25 μg/mL iron. The cells were incubated overnight, washed twice with 1 × PBS, and analyzed by flow cytometry (Guava EasyCyte™ Plus System; Millipore Corporation, Billerica, MA). Side scatter was measured and used as a marker for nanoparticles; cells with increased side scatter compared to control cells were counted as magnetic nanoparticle-loaded cells. The experiment was conducted in triplicate and 10,000 cells were analyzed for each replicate. Data were analyzed by using CytoSoft® software (Cytosoft 5.3; Guava EasyCyte Plus System; Millipore).

MTT assay

Thiazolyl blue was dissolved in PBS at 5 mg/mL to give the reagent solution. MTT buffer solution was prepared as 10% (weight/volume) sodium dodecyl sulfate and 0.1 M hydrochloric acid in water. To assay cell viability, the reagent solution was added 1:10 to the cell medium and the cells were placed back into the incubator. After 4 hours, the MTT buffer solution was added 1:1 to the medium and the plates were placed back into the incubator overnight. After incubating, the absorbance at 550 nm and 690 nm was recorded. Quantity ($absorbance_{550\ nm} - absorbance_{690\ nm}$) was calculated and the control value was scaled to 100% cell viability.

Tumor homing

To test the homing ability of Mo/Ma cells on Pan02 tumors, 7×10^5 Pan02 cells were injected i.p. to two mice on day zero. On day four, 1×10^6 PKH26 red fluorescent dye labeled Mo/Ma cells were injected i.p. (manufacturer's instructions were followed for PKH26 labeling). Mice were euthanized on day seven and day ten, and tissues (mesentery/tumor, kidney, liver, spleen, lung) collected and fixed in buffered neutral formalin. Twenty-four hours after fixation, tissues were incubated in sucrose gradient and snap frozen. Five to eight micron sections were made and stained with Hoechst for nuclear counterstaining; serial sections were stained with hematoxylin and eosin.

To verify that Mo/Ma cells were within Pan02 tumors, 7×10^5 Pan02 cells expressing firefly luciferase intracellularly were injected i.p. to five mice on day zero. On day 13, 1×10^6 Hoechst-labeled Mo/Ma cells were loaded with magnetic nanoparticles and injected i.p. Mice were euthanized on day 17 and tissues were snap-frozen. Five to eight micron sections were prepared by cryostat sectioning and stained with rabbit α-firefly luciferase antibody and DyLight® 650 conjugated sheep α-rabbit IgG antibody (Abcam, Cambridge, MA).

Magnetic heating apparatus to generate AMF

The AMF was generated by a converted 10 kW commercial inductive heater (Superior Induction Company, Pasadena, CA). In these experiments, only 1.5 kW power was used to produce 145 kHz sinusoidal AMF in a copper coil. (The power absorption of magnetic nanoparticles from AMF strongly increases with the frequency. This would suggest that higher frequency is desirable to produce better effects for magnetic hyperthermia treatment. In addition to the absorption of the magnetic nanoparticles, the tissue also absorbs energy from the magnetic field. This latter effect is also a strong function of the frequency. The optimum value of the frequency has been found to be around ~100 kHz).[52] The magnetic field intensity was calculated to be approximately 0.05 Tesla. The four-turn 1″ diameter coil was coated with silver and water cooled to eliminate residual heating effects from the resistive loss. The diameter of the coil was chosen to facilitate the complete inclusion of mice in a perforated plastic tube inside the coil.

Intratumoral nanoparticle heat generation

Six C57BL/6 mice (11 weeks old) were injected with 700,000 Pan02 cells in 100 μL PBS subcutaneously. To create a model for intratumoral heat generation by the loaded Mo/Ma, 21 days later, when tumors were palpable, 1,000,000 Mo/Ma loaded with nanoparticles were injected in 10 μL PBS intratumorally to three of the mice. The other three mice received 1,000,000 unloaded Mo/Ma in 10 μL PBS intratumorally. After injections, the mice were euthanized and the tumors were removed. The temperature of the tumors

was recorded using an infrared camera (FLIR, Boston, MA). The tumors were then exposed to AMF for 15 minutes and the temperature of the tumors was again measured using the infrared camera. The difference in temperature before and after AMF was calculated and the loaded and unloaded monocyte groups were compared.

In vivo experiment

C57BL/6 mice (11 weeks old) were injected with 700,000 Pan02 cells in 100 µL PBS i.p. on day zero to generate a murine model of disseminated pancreatic cancer. These mice were then randomly divided into five groups as follows: (1) tumor control; (2) Mo/Ma control; (3) nanoparticle control; (4) AMF control; and (5) AMF treatment.

On day five, 2×10^6 Mo/Ma loaded with nanoparticles were injected in 100 µL PBS i.p. to groups three (nanoparticle control) and five (AMF treatment). Groups two (Mo/Ma control) and four (AMF control) also received 2×10^6 Mo/Ma which were not loaded. Group one (tumor control) received 100 µL PBS i.p. This procedure was repeated on days nine and 13.

On day eight, mice from groups four (AMF control) and five (AMF treatment) were anesthetized with isoflurane and exposed to an AMF for 20 minutes. This procedure was repeated on days 12 and 16.

After three rounds of treatments, the mice were closely observed and allowed to continue until they displayed signs of clinical symptoms of cancer, at which point they were euthanized using carbon dioxide, and the tumors were collected and weighed (Figure 2).

Duration of clinical symptoms

The measured outcome for this study was mouse survival. To minimize potential pain and distress of the mice, however, a system was developed that allowed euthanasia of the mice shortly before they died. The mice were scored numerically one to five based on the body condition of the mice (primarily the spine and dorsal pelvic bone prominence) with a score of three indicative of a healthy mouse. This initial score was then modified by the presence of extreme lethargy, dehydration, ataxia, head tilt, severe hunching, limb dragging, severe raised hair, Harderian gland secretions, ascites, labored breathing, or bloody tail. Pronounced symptoms led to a subtraction of one point from the body condition score, while mild cases led to the addition of a "minus symbol" to the score (eg, three–). The mice were scored by this system every 12 hours, and any mouse that scored two or less was euthanized and the day/time recorded. The euthanasia day/time data were then treated like survival data and modeled using Kaplan–Meier statistics to determine the statistical significance of the data.

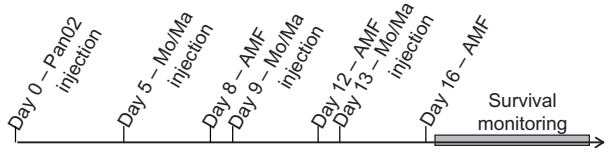

Figure 2 Treatment cycle for the in vivo study.
Abbreviations: AMF, alternating magnetic field; Mo/Ma, monocyte/macrophage-like cells.

Results

Toxicity and loading of nanoparticles

The nanoparticles did not show any toxicity at concentrations less than 100 µg/mL iron, although some slight toxicity was shown at 100 µg/mL and 200 µg/mL iron (Figure 3A). Mo/Ma took up the nanoparticles in a manner proportional to the iron concentration (Figure 3B). The percentage of cells containing nanoparticles (defined as cells that exhibit increased side scatter after loading) also increased in a manner proportional to the iron concentration (Figure 3C). Based on these results, to prevent undesired toxicity while maximizing the amount of iron loaded, nanoparticles were loaded at 37.5 µg/mL iron for the in vivo experiment. To determine the exact amount of iron loaded in the cells for the in vivo experiment, when Mo/Ma were lifted for the in vivo experiment, excess cells were collected and iron content was measured using the ferrozine assay. The iron content of Mo/Ma injected was 2.12 ± 0.37 pg iron/cell or 4.25 ± 0.74 µg iron/2,000,000 cells.

Tumor homing studies

To determine if Mo/Ma would home to Pan02 tumors, two mice bearing i.p. Pan02 tumors were injected i.p. with PKH26-labeled Mo/Ma. Three days after injection, the first mouse was euthanized. Tissue imaging showed that the Mo/Ma effectively homed to the tumor, but did not infiltrate other organs, including the pancreas, spleen, liver, and kidney. At 6 days, the second mouse was sacrificed and tissue imaging showed again that the monocyte-like cells penetrated tumor tissue but not healthy tissue (Figure 4).

Hematoxylin and eosin staining of serial sections demonstrate that the tissue to which the Mo/Ma home is highly disorganized, indicative of tumor tissue (Figure 5A and B). To further verify that the Mo/Ma were, in fact, in tumor tissue, five mice bearing i.p. Pan02 tumors expressing firefly luciferase were injected i.p. with Mo/Ma which were loaded

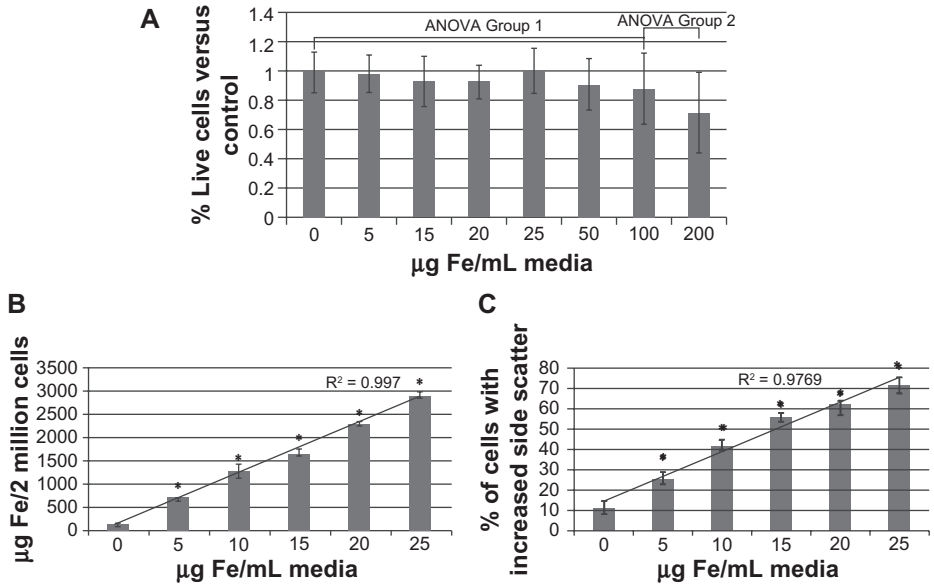

Figure 3 Nanoparticle loading. Monocyte/macrophage-like cells were cultured overnight in increasing concentrations of nanoparticles. The next morning cells were washed and assayed. (**A**) Toxicity of nanoparticles: cells were assayed for viability using 3-(4,5-Dimethylthiazol-2-yl)-2,5-diphenyltetrazolium bromide assay. (**B**) Loading of nanoparticles: cells were assayed for iron content using the ferrozine assay. (**C**) Percent of cells loaded: cells were assayed for increased side scatter using flow cytometry.
Note: Error bars are standard deviation. *= $P < 0.05$.
Abbreviations: ANOVA, analysis of variance; Fe, iron.

with Hoechst and magnetic nanoparticles. Four days after injection, the mice were euthanized. Antibody staining for firefly luciferase demonstrated that Mo/Ma were in tumor tissue (Figure 5C).

Nanoparticle heating of tumors

To verify that the cell-delivered nanoparticles could cause significant heating of the tumor, a subcutaneous Pan02 model was generated. (The subcutaneous model was used to give more accessible tumors for measurement purposes). The temperature change caused by AMF induced hyperthermia using the nanoparticle-loaded Mo/Ma was 4.0°C ± 0.7°C after 15 minutes of AMF exposure, or moderate hyperthermia. As a comparison, the temperature change using the unloaded Mo/Ma was 1.0°C ± 0.5°C (Figure 6, $P = 0.0056$).

Mouse survival

To determine the effectiveness of the treatment, Pan02 tumors were given i.p. to C57BL/6 mice and the mice were treated as described in the methods section. The euthanasia data were collected and modeled using Kaplan–Meier survival statistics. The data are reported as days subsequent to tumor injection (day zero) (Figure 7). The Kaplan–Meier test showed that the survival curves were significantly different ($P < 0.005$). All of the mice from the tumor control group were euthanized due to clinical symptoms (hereafter referred to as "succumbed") by day 23. Similarly all of the Mo/Ma control mice succumbed by day 25, all of the nanoparticle control mice succumbed by day 26, and all of the AMF control mice succumbed by day 25. Modeling with Kaplan–Meier statistics showed no significant difference between any of these groups. The AMF treatment mice survived substantially longer, with mice lasting until 33.5 days. The survival of the AMF treatment group was shown to be significant against all control groups ($P < 0.005$ for all comparisons). The average increase in survival versus tumor control for the AMF treatment group was 7 days, a 31% increase in life expectancy post-tumor insertion.

Discussion

It has been shown here for the first time that tumor-homing cells specifically delivering magnetic nanoparticles for AMF therapy can significantly prolong the lives of mice bearing deep and disseminated i.p. pancreatic tumors. Paramagnetic core/shell iron/iron oxide magnetic nanoparticles were surface modified for low toxicity therapeutic use. These magnetic nanoparticles were loaded into Mo/Ma cells, which were demonstrated to be tumor homing cells. The Mo/Ma cells were injected i.p. into tumor-bearing mice and trafficked specifically to the tumor. Three days later, the mice were exposed to AMF, which caused the nanoparticles to generate heat, leading to localized hyperthermia.

It was found that the Mo/Ma homed effectively to the pancreatic tumors after i.p. administration. This is not surprising,

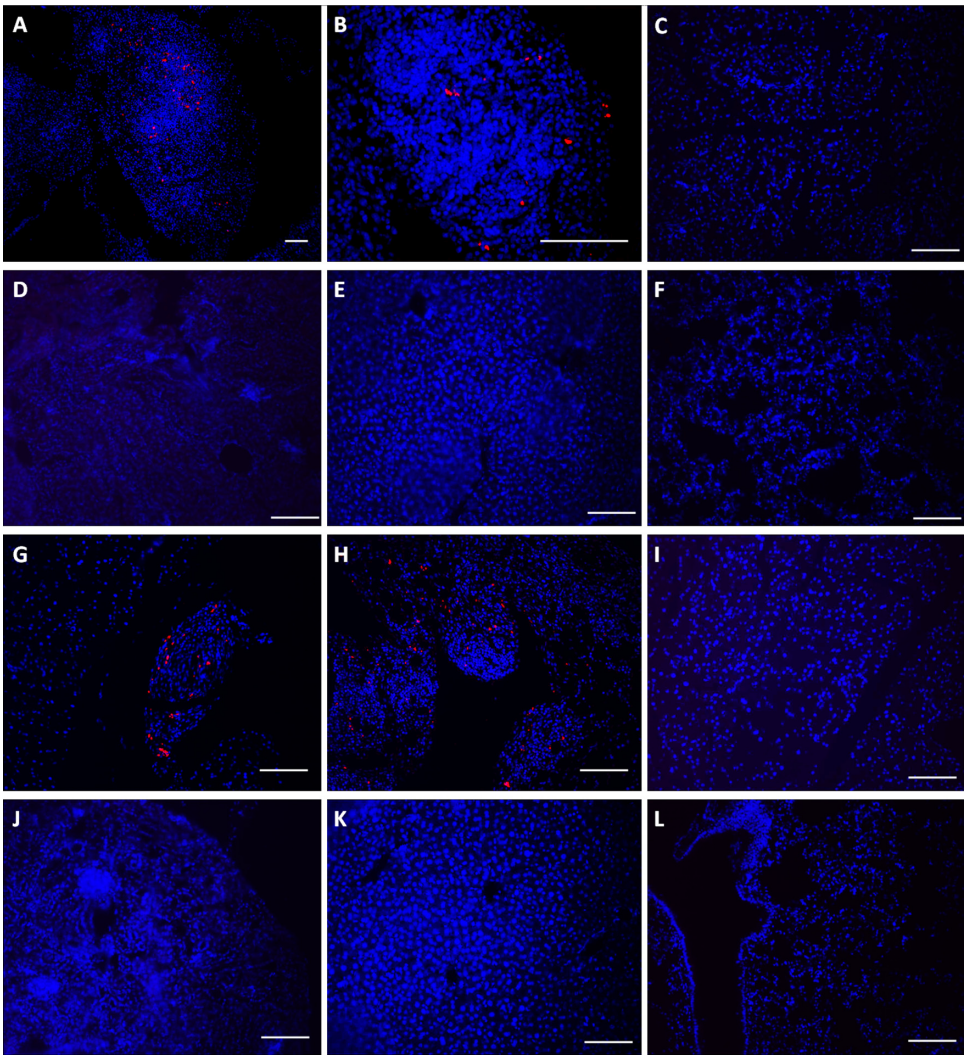

Figure 4 Monocyte/macrophage-like cells (Mo/Ma) only infiltrate Pan02 tumors. PKH26-labeled Mo/Ma were injected intraperitoneally into mice bearing intraperitoneal Pan02 tumors. (**A**)–(**F**) Mice were euthanized 3 days after Mo/Ma injection and organs were harvested and imaged for PKH26 (Mo/Ma). Representative images are shown. (**A**) Tumor 10×; (**B**) tumor 40×; (**C**) pancreas; (**D**) kidney; (**E**) liver; and (**F**) lung. (**G**–**L**) Mice were euthanized 6 days after Mo/Ma injection and organs were harvested and imaged for PKH26 (Mo/Ma). Representative images are shown. (**G**) Tumor (note healthy pancreas at the top left); (**H**) tumor; (**I**) pancreas; (**J**) kidney; (**K**) liver; and (**L**) lung.

Notes: Blue = Hoechst nuclear counterstain; red = PKH26 (Mo/Ma). All scale bars are 100 μm, objective is 20× unless otherwise specified.

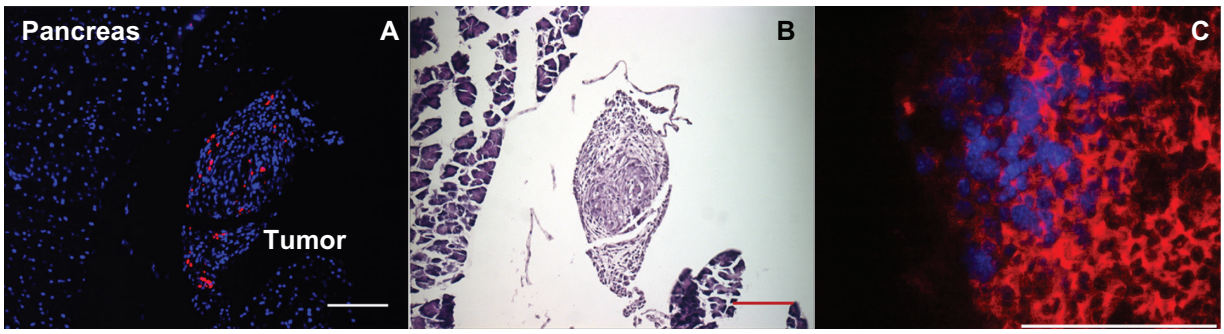

Figure 5 Monocyte/macrophage-like cells (Mo/Ma) infiltrate Pan02 tumors. (**A** and **B**) Mo/Ma loaded with PKH26 were injected into mice bearing intraperitoneal Pan02 tumors. Six days later mice were euthanized and tumors were harvested. (**A**) Hoechst nuclear counterstained section shows Mo/Ma labeled with PKH26 in tumor. (**B**) Hematoxylin and eosin staining of serial sections shows irregular morphology demonstrating that the targeted area is a tumor. Scale bars = 100 μm. (**C**) Mo/Ma labeled with Hoechst before injection were injected into mice bearing Pan02 expressing firefly luciferase tumors. Five days later mice were euthanized and tumors were harvested. Sections were stained with rabbit α-firefly luciferase and DyLight® 650-goat α-rabbit (Abcam, Cambridge, MA) (sections were not counterstained with Hoechst). Immunohistochemistry verifies that the Mo/Ma infiltrate pancreatic tumors.

Notes: (A) Blue = Hoechst; red = PKH26 (Mo/Ma), (C) Blue = Hoechst (Mo/Ma); red = DyLight® 650 (Pan02 cells). Scale bar = 100 μm.

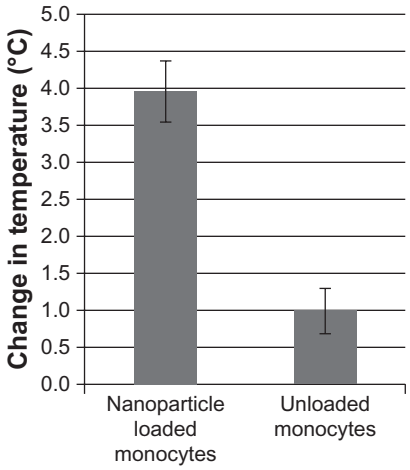

Figure 6 Heat generation by nanoparticle-loaded monocyte/macrophage-like cells.

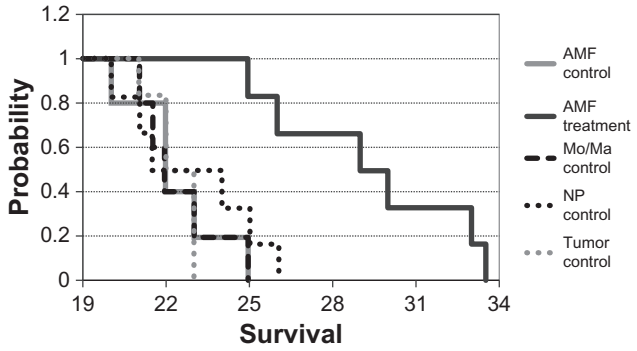

Figure 7 Duration to clinical symptoms ("survival").
Notes: Mice were treated and monitored as described. Mice were euthanized when they displayed clinical signs of cancer and the day/time was recorded (n = 5 or 6 for each group). $P < 0.005$ for alternating magnetic field treatment versus all other groups.
Abbreviations: AMF, alternating magnetic field; Mo/Ma, monocyte/macrophage-like cells; NP, nanoparticle.

because monocytes and/or macrophages are often found as tumor-associated cells. Rat monocytes were shown to efficiently invade rat glioma spheroids in vitro and peritoneal macrophages specifically migrated to rat gliomas after intravenous or intracarotid administration.[39,40] Interestingly, in this case, the mouse monocytes physically migrated only to the tumors within the peritoneal cavity, while normal tissues did not contain monocytes.

Classically, hyperthermia kills tumor tissue by heating proteins and other macromolecules to the point of denaturing faster than the cell can renature them. Since the system demonstrated here was substantially effective with only 4 µg of iron injected into the mouse per treatment cycle, other mechanisms of action may be present. The nanoparticle control group demonstrates that the nanoparticles themselves do not have any treatment value; similarly, the AMF control group demonstrates that AMF treatment does not have any stand-alone value. The Mo/Ma control group demonstrates that the Mo/Ma neither increase nor decrease tumor growth. Thus, AMF activation of the magnetic nanoparticles is primarily responsible for the effect. Low grade hyperthermia has been shown to recruit various immune cells, including dendritic cells, natural killer cells, neutrophils, and cytotoxic T cells.[53–61] Although future studies are needed, this or another similar mechanism may have greatly increased the effectiveness of the treatment and could explain why such a low dose of magnetic nanoparticles can effect such a large survival advantage. The authors are currently investigating potential

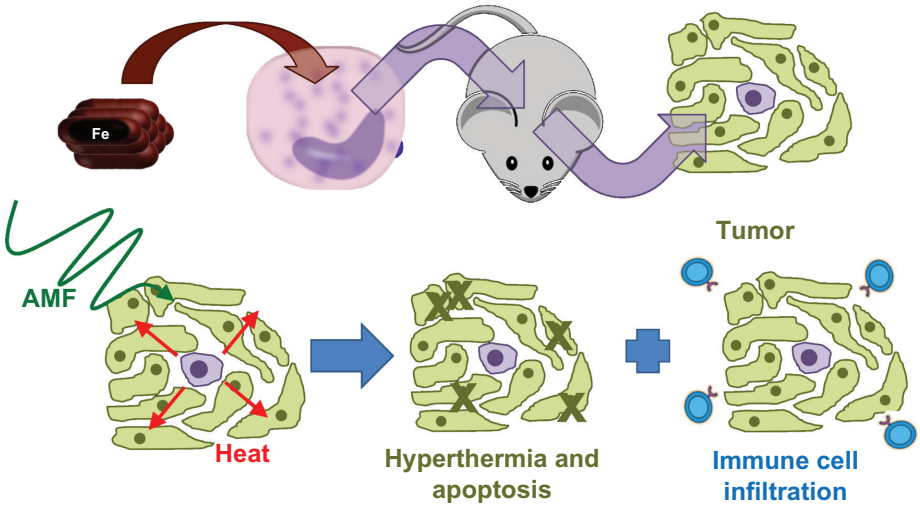

Figure 8 Model of the demonstrated system.
Notes: First, nanoparticles were loaded into monocyte/macrophage-like cells by inclusion in medium. The monocyte/macrophage-like cells were then injected intraperitoneally into mice bearing intraperitoneal Pan02 tumors and they specifically homed to the tumors. Three days after injecting the cells, the mice were exposed to an alternating magnetic field, which caused the nanoparticles to generate heat, leading to hyperthermia.
Abbreviations: AMF, alternating magnetic field; Fe, iron.

mechanisms involved in mediating survival extension, and those results will be described in a subsequent report.

Conclusion

In this report, the development of a localized hyperthermia treatment using tumor-tropic Mo/Ma to deliver magnetic nanoparticles for AMF activation has been described (Figure 8). The system described here holds potential for further development as a specific delivery method for magnetic nanoparticle-generated localized hyperthermia for targeted therapy of pancreatic and other types of cancer.

Acknowledgments

This publication was made possible by NIH grant P20 RR016475 from the INBRE Program of the National Center for Research Resources. The authors would also like to thank the Kansas Bioscience Authority and the National Institutes of Health (NIH grant 1R21CA135599 and NIH-COBRE grant P20 RR0117686) for supporting this work.

Disclosure

The authors report no conflicts of interest in this work.

References

1. Philip PA, Mooney M, Jaffe D, et al. Consensus report of the national cancer institute clinical trials planning meeting on pancreas cancer treatment. *J Clin Oncol*. 2009;27(33):5660–5669.
2. Hildebrandt B, Wust P, Ahlers O, et al. The cellular and molecular basis of hyperthermia. *Crit Rev Oncol Hematol*. 2002;43(1):33–56.
3. Shecterle LM, St Cyr JA. Whole body hyperthermia as a potential therapeutic option. *Cancer Biother*. 1995;10(4):253–256.
4. Hildebrandt B, Hegewisch-Becker S, Kerner T, et al; German Interdisciplinary Working Group on Hyperthermia. Current status of radiant whole-body hyperthermia at temperatures >41.5 degrees C and practical guidelines for the treatment of adults. *Int J Hyperthermia*. 2005;21(2):169–183.
5. Habash RW, Bansal R, Krewski D, Alhafid HT. Thermal therapy, part 2: hyperthermia techniques. *Crit Rev Biomed Eng*. 2006;34(6):491–542.
6. Sminia P, van der Zee J, Wondergem J, Haveman J. Effect of hyperthermia on the central nervous system: a review. *Int J Hyperthermia*. 1994;10(1):1–30.
7. Vertree RA, Leeth A, Girouard M, Roach JD, Zwischenberger JB. Whole-body hyperthermia: a review of theory, design and application. *Perfusion*. 2002;17(4):279–290.
8. Jia D, Liu J. Current devices for high-performance whole-body hyperthermia therapy. *Expert Rev Med Devices*. 2010;7(3):407–423.
9. Kraybill WG, Olenki T, Evans SS, et al. A phase I study of fever-range whole body hyperthermia (FR-WBH) in patients with advanced solid tumours: correlation with mouse models. *Int J Hyperthermia*. 2002;18(3):253–266.
10. Jia D, Rao W, Wang C, et al. Inhibition of B16 murine melanoma metastasis and enhancement of immunity by fever-range whole body hyperthermia. *Int J Hyperthermia*. 2011;27(3):275–285.
11. Ai J, Biazar E, Jafarpour M, et al. Nanotoxicology and nanoparticle safety in biomedical designs. *Int J Nanomedicine*. 2011;6:1117–1127.
12. Chen B, Wu W, Wang X. Magnetic iron oxide nanoparticles for tumor-targeted therapy. *Curr Cancer Drug Targets*. 2011;11(2):184–189.
13. Soenen SJ, Himmelreich U, Nuytten N, De Cuyper M. Cytotoxic effects of iron oxide nanoparticles and implications for safety in cell labelling. *Biomaterials*. 2011;32(1):195–205.
14. Suh JS, Lee JY, Choi YS, et al. Efficient labeling of mesenchymal stem cells using cell permeable magnetic nanoparticles. *Biochem Biophys Res Commun*. 2009;379(3):669–675.
15. Trahms L, Fannin PC, Kotitz R. Time domain study of Brownian and Neel relaxation in ferrofluids. *J Magn Magn Mater*. 1995;149(1–2):42–46.
16. Pakhomov AB, Bao Y, Krishnan KM. Effects of surfactant friction on Brownian magnetic relaxation in nanoparticle ferrofluids. *J Appl Phys*. 2005;97(10):10Q305/301–310Q305/303.
17. Shapiro MG, Atanasijevic T, Faas H, Westmeyer GG, Jasanoff A. Dynamic imaging with MRI contrast agents: quantitative considerations. *Magn Reson Imaging*. 2006;24(4):449–462.
18. Shinkai M, Yanase M, Suzuki M, et al. Intracellular hyperthermia for cancer using magnetite cationic liposomes. *J Magn Magn Mater*. 1999;194(1–3):176–184.
19. Le B, Shinkai M, Kitade T, et al. Preparation of tumor-specific magnetoliposomes and their application for hyperthermia. *J Chem Eng Jpn*. 2001;34(1):66–72.
20. Ito A, Shinkai M, Honda H, et al. Heat shock protein 70 expression induces antitumor immunity during intracellular hyperthermia using magnetite nanoparticles. *Cancer Immunol Immunother*. 2003;52(2):80–88.
21. Jordan A, Scholz R, Maier-Hauff K, et al. The effect of thermotherapy using magnetic nanoparticles on rat malignant glioma. *J Neurooncol*. 2006;78(1):7–14.
22. Jordan A, Scholz R, Wust P, et al. Effects of magnetic fluid hyperthermia (MFH) on C3H mammary carcinoma in vivo. *Int J Hyperthermia*. 1997;13(6):587–605.
23. Jordan A, Scholz R, Wust P, et al. Endocytosis of dextran and silan-coated magnetite nanoparticles and the effect of intracellular hyperthermia on human mammary carcinoma cells in vitro. *J Magn Magn Mater*. 1999;194(1–3):185–196.
24. Hilger I, Andra W, Hergt R, Hiergeist R, Schubert H, Kaiser WA. Electromagnetic heating of breast tumors in interventional radiology: in vitro and in vivo studies in human cadavers and mice. *Radiology*. 2001;218(2):570–575.
25. Johannsen M, Thiesen B, Jordan A, et al. Magnetic fluid hyperthermia (MFH) reduces prostate cancer growth in the orthotopic Dunning R3327 rat model. *Prostate*. 2005;64(3):283–292.
26. Ohno T, Wakabayashi T, Takemura A, et al. Effective solitary hyperthermia treatment of malignant glioma using stick type CMC-magnetite. In vivo study. *J Neurooncol*. 2002;56(3):233–239.
27. Kawai N, Futakuchi M, Yoshida T, et al. Effect of heat therapy using magnetic nanoparticles conjugated with cationic liposomes on prostate tumor in bone. *Prostate*. 2008;68(7):784–792.
28. Krishnan S, Diagaradjane P, Cho SH. Nanoparticle-mediated thermal therapy: evolving strategies for prostate cancer therapy. *Int J Hyperthermia*. 2010;26(8):775–789.
29. Aboody KS, Brown A, Rainov NG, et al. Neural stem cells display extensive tropism for pathology in adult brain: evidence from intracranial gliomas. *Proc Natl Acad Sci U S A*. 2000;97(23):12846–12851.
30. Arbab AS, Pandit SD, Anderson SA, et al. Magnetic resonance imaging and confocal microscopy studies of magnetically labeled endothelial progenitor cells trafficking to sites of tumor angiogenesis. *Stem Cells*. 2006;24(3):671–678.
31. De Palma M, Mazzieri R, Politi LS, et al. Tumor-targeted interferon-alpha delivery by Tie2-expressing monocytes inhibits tumor growth and metastasis. *Cancer Cell*. 2008;14(4):299–311.
32. Ganta C, Chiyo D, Ayuzawa R, et al. Rat umbilical cord stem cells completely abolish rat mammary carcinomas with no evidence of metastasis or recurrence 100 days post-tumor cell inoculation. *Cancer Res*. 2009;69(5):1815–1820.
33. Nakamizo A, Marini F, Amano T, et al. Human bone marrow-derived mesenchymal stem cells in the treatment of gliomas. *Cancer Res*. 2005;65(8):3307–3318.

34. Rachakatla RS, Marini F, Weiss ML, Tamura M, Troyer D. Development of human umbilical cord matrix stem cell-based gene therapy for experimental lung tumors. *Cancer Gene Ther*. 2007;14(10):828–835.
35. Rachakatla RS, Pyle MM, Ayuzawa R, et al. Combination treatment of human umbilical cord matrix stem cell-based interferon-beta gene therapy and 5-fluorouracil significantly reduces growth of metastatic human breast cancer in SCID mouse lungs. *Cancer Invest*. 2008;26(7):662–670.
36. Studeny M, Marini FC, Champlin RE, Zompetta C, Fidler IJ, Andreeff M. Bone marrow-derived mesenchymal stem cells as vehicles for interferon-beta delivery into tumors. *Cancer Res*. 2002;62(13): 3603–3608.
37. Studeny M, Marini FC, Dembinski JL, et al. Mesenchymal stem cells: potential precursors for tumor stroma and targeted-delivery vehicles for anticancer agents. *J Natl Cancer Inst*. 2004;96(21):1593–1603.
38. Rachakatla R, Balivada S, Seo GM, et al. Attenuation of mouse melanoma by A/C magnetic field after delivery of bi-magnetic nanoparticles by neural progenitor cells. *ACS Nano*. 2010;4(12):7093–7104.
39. Solinas G, Germano G, Mantovani A, Allavena P. Tumor-associated macrophages (TAM) as major players of the cancer-related inflammation. *J Leukoc Biol*. 2009;86(5):1065–1073.
40. Strik HM, Hulper P, Erdlenbruch B, et al. Models of monocytic invasion into glioma cell aggregates. *Anticancer Res*. 2006;26(2A):865–871.
41. Matsui M, Shimizu Y, Kodera Y, Kondo E, Ikehara Y, Nakanishi H. Targeted delivery of oligomannose-coated liposome to the omental micrometastasis by peritoneal macrophages from patients with gastric cancer. *Cancer Sci*. 2010;101(7):1670–1677.
42. Muthana M, Giannoudis A, Scott SD, et al. Use of macrophages to target therapeutic adenovirus to human prostate tumors. *Cancer Res*. 2011;71(5):1805–1815.
43. Baek SK, Makkouk AR, Krasieva T, Sun CH, Madsen SJ, Hirschberg H. Photothermal treatment of glioma; an in vitro study of macrophage-mediated delivery of gold nanoshells. *J Neurooncol*. 2011;104(2): 439–448.
44. Doi C, Maurya DK, Pyle MM, Troyer D, Tamura M. Cytotherapy with naive rat umbilical cord matrix stem cells significantly attenuates growth of murine pancreatic cancer cells and increases survival in syngeneic mice. *Cytotherapy*. 2010;12(3):408–417.
45. Zhang G, Liao Y, Baker I. Surface engineering of core/shell iron/iron oxide nanoparticles from microemulsions for hyperthermia. *Mater Sci Eng C Mater Biol Appl*. 2010;30(1):92–97.
46. Zeng Q, Baker I, Loudis JA, Liao Y, Hoopes PJ, Weaver JB. Fe/Fe oxide nanocomposite particles with large specific absorption rate for hyperthermia. *Appl Phys Lett*. 2007;90(23):233112–233115.
47. Carpenter EE, Sims JA, Wienmann JA, Zhou WL, O'Connor CJ. Magnetic properties of iron and iron platinum alloys synthesized via microemulsion techniques. *J Appl Phys*. 2000;87(9):5615–5617.
48. Glavee GN, Klabunde KJ, Sorensen CM, Hadjipanayis GC. Chemistry of borohydride reducton of iron(II) and iron(III) ions in aqueous and non-aqueous media. Formation of nanoscale Fe, FeB and Fe2B powders. *Inorg Chem*. 1995;34(1):28–35.
49. Stuart H, Ridley N. Lattice parameters and Curie-point anomalies of iron-cobalt alloys. *J Phys D Appl Phys*. 1969;2(4):485–492.
50. Mefford OT, Saville S, Qi B. Controlled surface functionalization of iron-oxide nanoparticles for field responsive biomedical applications. *PMSE Reprints*. 2009;101:1569.
51. Hong R, Fischer NO, Emrick T, Rotello VM. Surface PEGylation and ligand exchange chemistry of FePt nanoparticles for biological applications. *Chem Mater*. 2005;17(18):4617–4621.
52. Jordan A, Wust P, Fahling H, John W, Hinz A, Felix R. Inductive heating of ferrimagnetic particles and magnetic fluids: physical evaluation of their potential for hyperthermia. *Int J Hyperthermia*. 1993;9(1):51–68.
53. Appenheimer MM, Chen Q, Girard RA, Wang WC, Evans SS. Impact of fever-range thermal stress on lymphocyte-endothelial adhesion and lymphocyte trafficking. *Immunol Invest*. 2005;34(3):295–323.
54. Calderwood SK, Theriault JR, Gong J. How is the immune response affected by hyperthermia and heat shock proteins? *Int J Hyperthermia*. 2005;21(8):713–716.
55. Chen T, Guo J, Yang M, Zhu X, Cao X. Chemokine-containing exosomes are released from heat-stressed tumor cells via lipid raft-dependent pathway and act as efficient tumor vaccine. *J Immunol*. 2011;186(4):2219–2228.
56. Fuggetta MP, Alvino E, Tricarico M, et al. In vitro effect of hyperthermia on natural cell-mediated cytotoxicity. *Anticancer Res*. 2000;20(3A):1667–1672.
57. Ito A, Honda H, Kobayashi T. Cancer immunotherapy based on intracellular hyperthermia using magnetite nanoparticles: a novel concept of "heat-controlled necrosis" with heat shock protein expression. *Cancer Immunol Immunother*. 2006;55(3):320–328.
58. Manjili MH, Wang XY, Park J, et al. Cancer immunotherapy: stress proteins and hyperthermia. *Int J Hyperthermia*. 2002;18(6):506–520.
59. Milani V, Noessner E. Effects of thermal stress on tumor antigenicity and recognition by immune effector cells. *Cancer Immunol Immunother*. 2006;55(3):312–319.
60. Segal BH, Wang XY, Dennis CG, et al. Heat shock proteins as vaccine adjuvants in infections and cancer. *Drug Discov Today*. 2006; 11(11–12):534–540.
61. Muthana M, Multhoff G, Pockley AG. Tumour infiltrating host cells and their significance for hyperthermia. *Int J Hyperthermia*. 2010;26(3): 247–255.